Wave Motion 49 (2012) 691–709

Contents lists available at SciVerse ScienceDirect

Wave Motion

journal homepage: www.elsevier.com/locate/wavemoti

Particle dynamics in the KdV approximation

Handan Borluk [a], Henrik Kalisch [b,*]

[a] Department of Mathematics, Isik University, Kumbaba Mevkii Sile, 34980, Turkey

[b] Department of Mathematics, University of Bergen, Postbox 7800, 5020 Bergen, Norway

ARTICLE INFO

Article history:
Received 19 October 2011
Received in revised form 23 April 2012
Accepted 27 April 2012
Available online 15 May 2012

Keywords:
Surface waves
Boussinesq scaling
KdV equation
Particle trajectories
Solitary waves
Soliton interaction

ABSTRACT

The KdV equation arises in the framework of the Boussinesq scaling as a model equation for waves at the surface of an inviscid fluid. Encoded in the KdV model are relations that may be used to reconstruct the velocity field in the fluid below a given surface wave. In this paper, velocity fields associated to exact solutions of the KdV equation are found, and particle trajectories are computed numerically. The solutions treated here comprise the solitary wave, periodic traveling waves, and the two-soliton solutions. For solitary waves and periodic traveling waves, approximate particle paths are found in closed form.

1. Introduction

The Korteweg–de Vries (KdV) equation is a model equation describing the evolution of long-crested waves at the surface of a body of fluid. The main assumptions on the waves to be represented by solutions of the KdV equation are that they be of small amplitude and long wavelength when compared to the undisturbed depth of the fluid, and that the wave motion be predominantly one-directional. The equation arises in a certain parameter regime called the Boussinesq scaling [1], and it is possible to find exact solutions of the KdV equation describing solitary and periodic water waves [2]. The equation also features closed-form solutions describing overtaking collisions of solitary waves which are found to be elastic in the sense that the solitary waves reemerge unscathed from the interaction, except for a phase shift [3]. The discovery of the elastic solitary-wave interaction subsequently led to the development of the inverse-scattering method for the solution of the initial-value problem associated to the KdV equation [4]. Since the equation is exactly solvable, one may think of it as a completely-integrable infinite-dimensional Hamiltonian system. As a matter of fact, the KdV equation serves as a paradigm for the use of the inverse-scattering method for constructing solutions of evolution equations of Hamiltonian type.

Since the discovery of the elastic interaction of solitary waves, an immense body of work has accumulated. The KdV equation has been used extensively in physical studies of surface and internal water waves, and for many other situations in mathematical physics [5]. The equation has also been studied a great deal from a mathematical vantage point. Examples of topics under study include the solution of the initial-value problem with various boundary conditions, stability of special solutions, and applications of the inverse-scattering method. However, it appears that one aspect of the KdV as a model equation for surface water waves, namely the connection between surface wave patterns and the underlying flow has not been given much attention so far.

* Corresponding author.
E-mail addresses: hborluk@isikun.edu.tr (H. Borluk), henrik.kalisch@math.uib.no (H. Kalisch).

0165-2125/$ – see front matter © 2012 Elsevier B.V. All rights reserved.
doi:10.1016/j.wavemoti.2012.04.007

In the present article, the focus is on particle trajectories in the fluid below a given surface wave. The KdV equation will be studied in the non-dimensional form

$$\eta_t + \eta_x + \frac{3}{2}\eta\eta_x + \frac{1}{6}\eta_{xxx} = 0, \tag{1.1}$$

which appears when the undisturbed depth h_0 is taken as a unit of distance, and $\sqrt{h_0/g}$ is taken as a unit of time. Careful examination of the derivation of the equation as a surface water-wave model shows that it is possible to reconstruct an approximation of the fluid velocity field underneath the surface. In particular, it is possible to derive formulas expressing the horizontal and vertical velocity components in terms of the principal unknown variable η which describes the shape of the free surface. The most straightforward observation is that to first order in the perturbation parameter, the horizontal velocity u is independent of the depth at which it is measures, and we have $u = \eta$. However, since the KdV equation is valid to second order, this relation may be improved to read

$$u = \eta - \frac{1}{4}\eta^2 + \frac{1}{3}\eta_{xx}, \tag{1.2}$$

which holds to second-order [6]. In the relation (1.2) u denotes the horizontal velocity at the flat bottom. However, it is also possible to find an expression for the horizontal velocity at an arbitrary depth in the fluid column. This development is already implicitly contained in the derivation presented in [6], and has also been exploited recently in the derivation and study of a general system of Boussinesq equations [7,8]. Once the velocity field associated to a surface wave has been found, one may study a number of important dynamic properties of the flow, and in particular, one may construct approximate descriptions of the paths traced out by fluid particles below the surface.

Since the KdV equation is valid asymptotically in the limit of small amplitude and long wavelength, our results are of approximate character, and should only be applied for waves of small amplitude, and long wavelength. This stands in contrast to recent major advances in the study of particle motion in the full Euler equations. In particular, Constantin [9] showed that particle paths are not closed in periodic traveling-wave solutions of the full Euler system with free-surface boundary conditions. In [10], Constantin and Escher analyzed particle paths associated to solitary-wave solutions of the water-wave problem, and used maximum principles for elliptic operators to prove qualitative results about the particle velocities and trajectories.

On the other hand, asymptotic results have also been obtained for the case of small amplitude but arbitrary wavelength. Indeed, Constantin et al. [11] and Constantin and Villari [12], studied particle trajectories in the linearized water-wave problem, and proved mathematically that these trajectories are not closed. Results of this type are known in the engineering literature as Stokes drift, but mathematical proofs had not been available before they were given in [11,12]. A review of mathematical results about particle paths in the linearized water-wave problem is given by Ehrnström and Villari [13]. Numerical work was recently published by Chang et al. [14] who analyzed particle paths in deep-water waves in the Lagrangian framework.

It should also be mentioned that in order to approximate the velocity field beneath a solitary or periodic traveling wave, one may use a direct approximation of the wave structure, without going through the Boussinesq scaling. For instance, Grimshaw [15] and Fenton [16] found high-order approximations of solitary waves which also allow the evaluation of the velocity field below the surface. More recently, particle paths due to periodic traveling waves were found to high accuracy, and compared to particle paths observed in wavetank experiments by Chen et al. [17]. Previous results which are in the spirit of the present study were obtained by Clamond [18], and more recently by Henry [19]. In these articles, different strategies were used to construct the velocity field in the fluid associated to a periodic cnoidal solution of the KdV equation. Approximations of particle paths based on the relation $u = \eta$ were studied in [20,21].

Finally, we would like to remark that the study of particle trajectories using approximate methods is justified by strong regularity results ensuring the a priori analyticity of the stream function, for both irrotational and rotational flows [22–25].

In the next section, the physical setup of the surface water wave problem is reviewed, and a short account of the derivation of the KdV equation is given. In Section 3, we use formulas such as (1.2) in connection with exact solutions to consider particle trajectories associated to surface solitary waves. In Section 4, particle paths in fluid flow below periodic surface waves are investigated. Finally, Section 5 features a study of particle paths associated to solitary-wave interactions. One important theme in Sections 3 and 4 is the comparison of approximate but closed-form expressions for particle paths to numerical approximations of the trajectories based on discretizing the governing ordinary differential equations. As will be shown, the numerical discretization – when used with a sufficiently small time step – yields a more reliable description of the particle trajectories than does any closed-form approximation. However, the latter may still be useful in cases where a quick estimate is desired.

2. Surface water waves and the Boussinesq scaling

The KdV equation is derived under the assumptions that the fluid is incompressible and inviscid. Furthermore, it is supposed that the fluid flow is irrotational and two-dimensional, and that the free surface can be described by a single-valued function $\eta(x, t)$. With these assumptions, the problem may be studied on the domain $\{(x, z) \in \mathbb{R} \times \mathbb{R} | 0 < z < h_0 + \eta(x, t)\}$

which extends to infinity in the positive and negative x-direction, and where the parameter h_0 represents the undisturbed depth of the fluid. On this domain, the two-dimensional Euler equations are given by

$$\begin{aligned} u_t + uu_x + vu_z &= -p_x, \\ v_t + uv_x + vv_z &= -p_z - g \end{aligned} \tag{2.1}$$

where (u, v) represents the velocity field, p denotes the pressure, g is the gravitational acceleration, and the density is assumed to be unity. The incompressibility of the fluid, and the irrotationality of the flow are expressed, respectively, by

$$u_x + v_z = 0 \quad \text{and} \quad u_z - v_x = 0. \tag{2.2}$$

The free-surface boundary conditions are given by requiring the pressure to be equal to atmospheric pressure at the surface if surface tension effects are neglected, and the kinematic boundary condition:

$$p = p_{atm} \quad \text{and} \quad \eta_t + u\eta_x = v, \quad \text{at } z = h_0 + \eta(x, t). \tag{2.3}$$

The geometric setup of the problem is illustrated in Fig. 1. Since the fluid is incompressible, and irrotational flow is assumed, it is customary to introduce a velocity potential $\phi(x, z, t)$. The surface-wave problem is then given in terms of the Laplace equation for ϕ, along with the nonlinear boundary conditions (2.3) on the free surface and the usual boundary condition at the bottom. The derivation of weakly nonlinear evolution equations of Boussinesq type is due to Boussinesq [1], and is thoroughly explained in [6,8]. The process relies on recognizing two parameters that describe the regime of waves with average amplitude a, and average wavelength λ. The parameter $\alpha = \frac{a}{h_0}$ then describes the relative amplitude of the waves, and the parameter $\beta = \frac{h_0^2}{\lambda^2}$ measures the 'shallowness' of the fluid in comparison to the wavelength. In [6], it is shown that to second-order accuracy in α and β, solutions of the free-surface problem described above may by approximated by solutions of the system

$$\begin{aligned} &\eta_t + h_0 w_x + (\eta w)_x - \frac{1}{6} h_0^3 w_{xxx} = 0, \\ &w_t + g\eta_x + w w_x - \frac{1}{2} h_0^2 w_{xxt} = 0, \end{aligned} \tag{2.4}$$

where w denotes the horizontal velocity at the bottom of the channel, and the potential is given to second order by $\phi = f - \frac{z}{2} f_{xx}$. The horizontal velocity at the bottom w is then given by the relation $w = f_x$. If the horizontal velocity is evaluated at a level $0 \le h_0\theta < h_0$, then in terms of the dependent variables η^θ and w^θ, the equations take the more general form

$$\eta_t^\theta + h_0 w_x^\theta + (\eta^\theta w^\theta)_x + \frac{1}{2}\left(\theta^2 - \frac{1}{3}\right) h_0^3 w_{xxx}^\theta = 0, \tag{2.5}$$

$$w_t^\theta + g\eta_x + w^\theta w_x^\theta - \frac{1}{2}\left(1 - \theta^2\right) h_0^2 w_{xxt}^\theta = 0. \tag{2.6}$$

The functions w and w^θ are related to second order in β by $w = w^\theta + \frac{1}{2}\theta^2 h_0^2 w_{xx}^\theta$. Using this relation, and differentiating the equation for ϕ gives the horizontal velocity at an arbitrary level in the fluid. This velocity is thus expressed by

$$u(x, z, t) = \phi_x = w^\theta(x, t) + \frac{1}{2}\left((h_0\theta)^2 - z^2\right) w_{xx}^\theta(x, t). \tag{2.7}$$

Similar considerations show that the vertical velocity can be written in terms of w^θ as

$$v(x, z, t) = -z\, w_x^\theta, \tag{2.8}$$

which is also correct to second order in β. Thus it is plain that the horizontal and vertical velocity components of the fluid at a point (x, z) can be expressed in terms of the horizontal velocity at a fixed height $h_0\theta$ from the even bottom.

As shown in [6], the KdV equation can be derived from (2.5) and (2.6) by assuming a certain relationship between w^θ and η which singles out waves that mainly travel in the direction of increasing values of x. This relation is given in dimensional form by

$$w^\theta = \frac{g}{c_0}\left\{\eta - \frac{1}{4h_0}\eta^2 + h_0^2\left(\frac{1}{3} - \frac{1}{2}\theta^2\right)\eta_{xx}\right\}, \tag{2.9}$$

and the corresponding KdV equation for η is

$$\eta_t + c_0\left(1 + \frac{3}{2h_0}\eta\right)\eta_x + \frac{h_0^2}{6} c_0 \eta_{xxx} = 0. \tag{2.10}$$

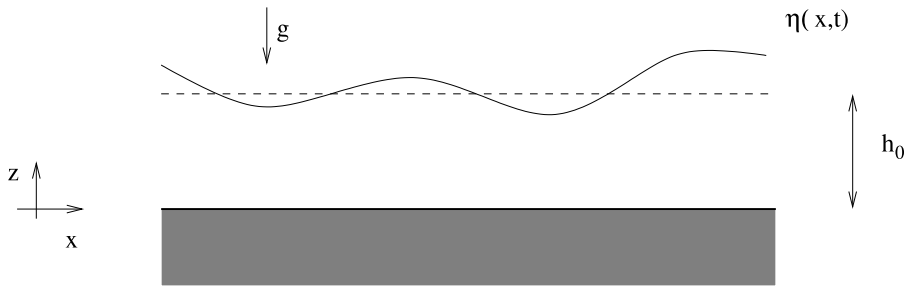

Fig. 1. The schematic elucidates the geometric setup of the problem. The free surface is described by a function $\eta(x, t)$. The undisturbed water depth is h_0, the gravitational acceleration is g, and the x-axis is aligned with the even bottom.

It now appears that (2.9) may be used in conjunction with (2.7) and (2.8) to reconstruct a velocity field associated to solutions of (2.10). This approximate velocity field is valid to the same order as the Eq. (2.10) describing the excursion of the free surface.

In the following, it will be convenient to define non-dimensional variables adapted to the problem at hand. In particular, the new variables are defined by

$$x \to h_0 x, \qquad z \to h_0 z, \qquad \eta \to h_0 \eta, \qquad t \to \frac{h_0}{c_0} t, \qquad w \to c_0 w.$$

The Eqs. (2.9) and (2.10) can be rewritten in terms of new variables as

$$w^\theta = \eta - \frac{1}{4}\eta^2 + \left(\frac{1}{3} - \frac{\theta^2}{2}\right)\eta_{xx}, \tag{2.11}$$

$$\eta_t + \left(1 + \frac{3}{2}\eta\right)\eta_x + \frac{1}{6}\eta_{xxx} = 0. \tag{2.12}$$

The expression (2.7) for the horizontal velocity of a fluid particle is given in non-dimensional variables as

$$u(x, z, t) = w^\theta(x, t) + \frac{1}{2}\left(\theta^2 - z^2\right) w^\theta_{xx}(x, t). \tag{2.13}$$

The relation (2.8) for the vertical velocity does not change under the nondimensionalization. It was indicated in [26], that values of θ close to but less than 1 could be advantageous if a close approximation to the linear dispersion relation of the water-wave problem is sought. In the context of particle paths it can be useful to set θ close to the initial z coordinate of the particle, so that a close representation is achieved. However, from the point of view of the Boussinesq scaling, all values of θ are formally equivalent. In practice, as long as the waves are within the validity of the Boussinesq scaling, the results will be qualitatively the same. The numerical computations which are presented in the following sections have been run with several values of θ, and the variation of the results has been minor in comparison to their main qualitative features.

3. Particle paths in solitary-wave solutions

In this section, our attention will be focused on the particle paths in the fluid due to the passage of a solitary wave at the surface. As is well known, the solitary-wave solution of the KdV equation is given by

$$\eta = \eta_0 \operatorname{sech}^2\left(\frac{\sqrt{3\eta_0}}{2}(x - x_0 - ct)\right), \tag{3.1}$$

where η_0 is the amplitude, x_0 is the initial location of the wave crest, and the phase velocity is given by

$$c = 1 + \frac{\eta_0}{2}. \tag{3.2}$$

In the following, we will always assume that the wavecrest is located at $x = 0$ at time $t = 0$, so that $x_0 = 0$. Defining the argument $\mathcal{A}(x, t) = \frac{\sqrt{3\eta_0}}{2}(x - ct)$, the relation (2.11) yields the expression

$$w^\theta = \eta_0 \operatorname{sech}^2(\mathcal{A})\left\{1 - \frac{\eta_0}{4}\operatorname{sech}^2(\mathcal{A}) - \frac{3}{2}\eta_0\left(\frac{1}{3} - \frac{\theta^2}{2}\right)\left(3\operatorname{sech}^2(\mathcal{A}) - 2\right)\right\} \tag{3.3}$$

for the horizontal velocity at $z = \theta$. For the solitary-wave solutions of the KdV equation, the horizontal and vertical velocities at an arbitrary point (x, z) in the fluid, and at a time t are then given by

$$\begin{aligned} u(x,z,t) &= \eta_0 \operatorname{sech}^2(\mathcal{A}) \left\{ 1 + \eta_0 - \frac{3}{2}\eta_0 z^2 + \frac{\eta_0}{4}(9z^2 - 7)\operatorname{sech}^2(\mathcal{A}) \right. \\ &\quad + \frac{3}{8}\eta_0^2 \left(\theta^2 - z^2\right)\left[35\operatorname{sech}^4(\mathcal{A}) - 34\operatorname{sech}^2(\mathcal{A}) \right. \\ &\quad \left. \left. + \ 4 - 3\theta^2\left(15\operatorname{sech}^4(\mathcal{A}) - 15\operatorname{sech}^2(\mathcal{A}) + 2\right)\right]\right\}, \\ v(x,z,t) &= -z\frac{\sqrt{3}}{2}\eta_0^{3/2}\tanh(\mathcal{A})\operatorname{sech}^2(\mathcal{A}) \\ &\quad \times \left\{ -2 + \eta_0\operatorname{sech}^2(\mathcal{A}) + 6\eta_0\left(\frac{1}{3} - \frac{\theta^2}{2}\right)\left(3\ \operatorname{sech}^2(\mathcal{A}) - 1\right)\right\}. \end{aligned}$$

Taking the functions $\xi(t)$ and $\zeta(t)$ to describe the x-coordinate and z-coordinate, respectively, of a particle originally located at the point $(x, z) = (\xi_0, \zeta_0)$, the particle motion is described by the differential equations

$$\frac{\partial \xi}{\partial t} = u\left(\xi(t), \zeta(t), t\right), \qquad \frac{\partial \zeta}{\partial t} = v\left(\xi(t), \zeta(t), t\right), \tag{3.4}$$

with initial conditions $\xi(0) = \xi_0$ and $\zeta(0) = \zeta_0$. These equations can be solved numerically. For instance, an efficient discretization of these equations can be effected by a four-stage Runge–Kutta method. It has been found in our numerical experiments that such a fourth-order method yields highly accurate results, even when used with a moderately small time step.

However, for some purposes it might be desirable to have available a closed-form expression which describes approximate particle paths. If it is assumed that the individual particles do not move a great deal during the passage of a solitary wave, the Eqs. (3.4) may be approximated by

$$\frac{\partial \bar{\xi}}{\partial t} = u(\xi_0, \zeta_0, t), \qquad \frac{\partial \bar{\zeta}}{\partial t} = v(\xi_0, \zeta_0, t), \tag{3.5}$$

where the initial position of the particle is again (ξ_0, ζ_0). Using these relations and the solutions of KdV equation given by (3.1) and (3.3) it is possible to find the expressions

$$\begin{aligned} \bar{\xi} &= X_0 - \frac{2}{\sqrt{3}\,c}\sqrt{\eta_0}\tanh(\mathcal{A}_0)\left\{1 - \frac{\eta_0}{6} + \frac{\eta_0}{12}\left(9\zeta_0^2 - 7\right)\operatorname{sech}^2(\mathcal{A}_0)\right. \\ &\quad \left. + \frac{3}{8}\eta_0^2\left(\theta^2 - \zeta_0^2\right)\operatorname{sech}^2(\mathcal{A}_0)\left[\operatorname{sech}^2(\mathcal{A}_0) + \left(2 - 3\theta^2\right)\left(3\ \operatorname{sech}^2(\mathcal{A}_0) - 1\right)\right]\right\}, \\ \bar{\zeta} &= Z_0 + \frac{\zeta_0}{c}\eta_0\operatorname{sech}^2(\mathcal{A}_0)\left\{1 - \frac{\eta_0}{4}\operatorname{sech}^2(\mathcal{A}_0) - \frac{3}{2}\eta_0\left(\frac{1}{3} - \frac{\theta^2}{2}\right)\left(3\ \operatorname{sech}^2(\mathcal{A}_0) - 2\right)\right\}. \end{aligned} \tag{3.6}$$

Here $\mathcal{A}_0$ represents the argument $\mathcal{A}_0(t) = \frac{\sqrt{3\eta_0}}{2}(\xi_0 - ct)$, corresponding to a solitary wave which is initially centered at $x = 0$, and a particle whose x-coordinate is initially $x = \xi_0$. The constants X_0 and Z_0 denote the difference between the initial particle location ξ_0 and ζ_0, respectively, and the expressions of the right-hand side evaluated at $t = 0$ (i.e. at $\mathcal{A}_0(0) = \frac{\sqrt{3\eta_0}}{2}(\xi_0)$).

In Figs. 2–4, sample particle paths are shown during the propagation of a surface solitary wave with amplitude $\eta_0 = 0.3$. In all figures in this article, the ordinate represents values of z unless indicated otherwise. Fig. 2 shows the time evolution of a fluid particle located in the surface. The wave profile is shown at $t = 0$ (light-gray), $t = 2$ (dark-gray) and $t = 4$ (black). The particle trajectory given by (3.6) is represented by the dashed curve. The particle location at the three instances where the wave profile is shown are color coded: the light-gray dot indicates the particle position at time $t = 0$; the dark-gray dot indicates the particle position at time $t = 2$; the black dot indicates the particle position at time $t = 4$. Similar color-coding is used in Figs. 3 and 4. As can be seen from these figures, fluid particles move to the right and upwards if they are located to the right of the crest. Particles located on the left of the crest move to the right and downwards. This is in agreement with the findings of Constantin and Escher [10]. It is also apparent that particles closer to the bed have smaller total excursion.

The particle trajectories shown as solid curves in the left panels of Figs. 3 and 4 are numerical approximations of solutions of (3.4) obtained with the 4-th order Runge–Kutta method mentioned above. In the right panel of Figs. 3 and 4, a comparison of the numerical approximation of particle trajectories using (3.4) and the explicit form (3.6) are shown (the approximate formula (3.6) is shown as a dashed curve). In this comparison, it is apparent that the approximation (3.6) yields particle paths that are somewhat shorter than the more accurate trajectories computed numerically. We also note in Fig. 4 that the horizontal displacement is independent of the initial depth of the particle if the approximation (3.6) is used. On the other hand, the horizontal displacement does depend on the initial depth of the particle as shown by the solid curves in the right

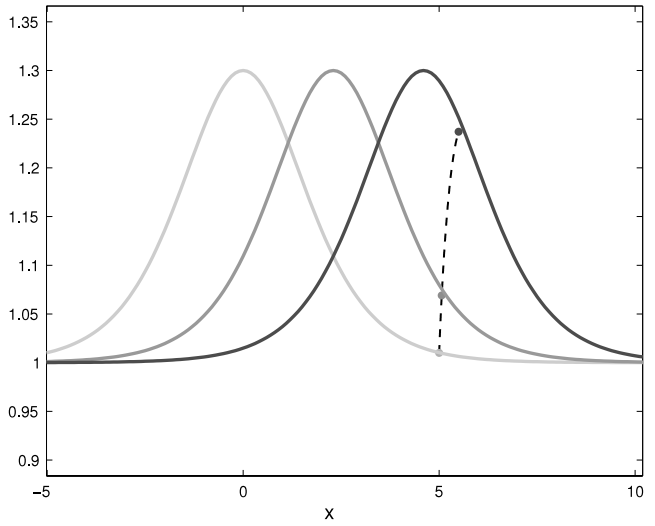

Fig. 2. The wave in the figure is shown at $t = 0$ (light-gray), $t = 2$ (dark-gray) and $t = 4$ (black). The dashed curve represents the path of a particle initially located in the surface at (5, 1.02). Note that the particle lags behind the surface, indicating that the approximation used in (3.6) yields a small error.

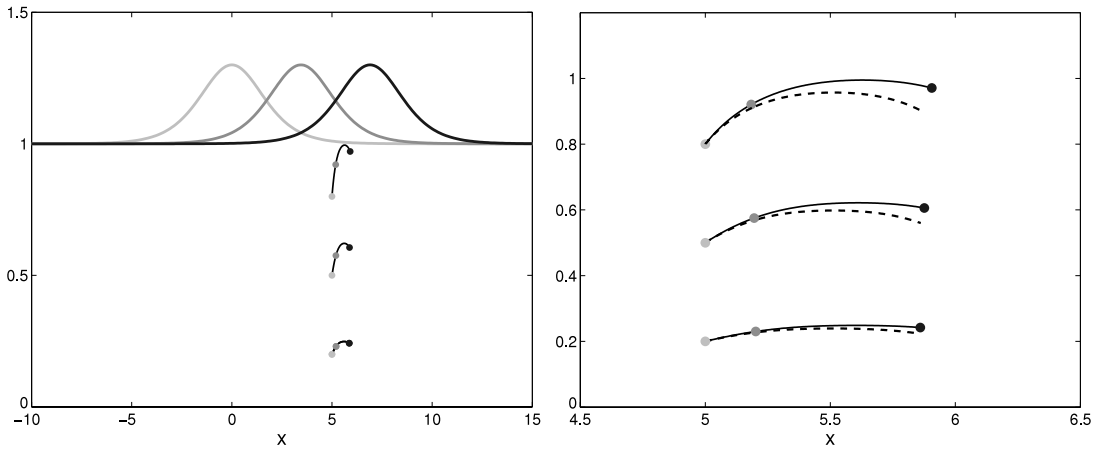

Fig. 3. The wave in the left panel is shown at $t = 0$ (light-gray), $t = 3$ (dark-gray) and $t = 6$ (black). The wave crest is initially located at $x = 0$. The paths of the fluid particles initially located at (5, 0.8), (5, 0.5) and (5, 0.2) are shown. The particle locations at the three instances where the wave profile is shown are color coded. The light-gray dots indicate the particle positions at time $t = 0$. The dark-gray dots indicate the particle positions at time $t = 3$. The black dots indicate the particle positions at time $t = 6$. The right panel features a comparison of the particle paths computed using the Runge–Kutta method (solid) and the approximate formula (3.6) (dashed).

panel of Fig. 4. The maximal possible excursion of a particle from rest into the vertical direction can be computed from (3.6) by setting $\xi_0 = 0$, and evaluating

$$\bar{\zeta}(t = 0) - \bar{\zeta}(t = -\infty) = \zeta_0 \frac{2\eta_0}{2 + \eta_0} \left[1 + \frac{3}{4}\eta_0 \left(\theta^2 - 1\right) \right],$$

where ζ_0 denotes the original z-coordinate of the particle. This expression confirms the decrease in total vertical excursion with increasing depths which was observed in Fig. 4. Of course such a behavior might be expected since particle amplitudes decay exponentially towards the bottom in the case of linear waves.

The mass flux due to the passage of a solitary wave can be computed from (3.6) by evaluating the following expression:

$$\bar{\xi}(t = \infty) - \bar{\xi}(t = -\infty) = \frac{4\sqrt{\eta_0}}{\sqrt{3}} \frac{1 - \frac{\eta_0}{6}}{1 + \frac{\eta_0}{2}}. \tag{3.7}$$

Since the nondimensional depth of the fluid is 1, this formula represents the total mass flux through a vertical cross-section in the fluid due to the passage of a solitary wave. Note that the mass flux due to the passage of a solitary waves can also be computed by observing that the KdV equation (1.1) is actually a mass conservation equation. Accordingly, the quantity

$$q_M = \eta + \frac{3}{4}\eta^2 + \frac{1}{6}\eta_{xx}$$

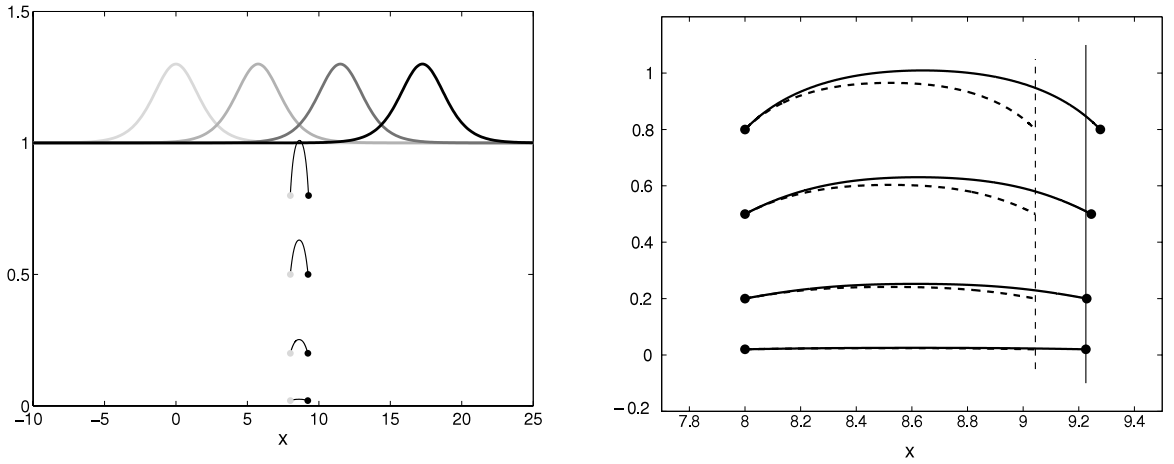

Fig. 4. The wave in the left panel is shown at $t = 0, t = 5, t = 10$ and $t = 15$. The paths of the particles initially located at (5, 0.8), (5, 0.5), (5, 0.2) (5, 0.01) are shown. The light-gray dots indicate the particle positions at time $t = 0$, and the black dots indicate the particle positions at time $t = 6$. The curves show the trajectories traced out by particles during the full passage of a solitary wave from the far field on the left to the right. The right panel features a comparison of the particle paths computed using the Runge–Kutta method (solid) and the approximate formula (3.6) (dashed). The vertical lines illustrate the final horizontal position of the lowest particle computed numerically (solid), and with the approximate formula (3.6) (dashed).

can be interpreted as the mass flux due to the wave motion. Therefore, the total mass flux due to a solitary wave can be computed by evaluating the integral

$$\begin{aligned} \mathcal{Q} &= \int_{-\infty}^{\infty} q_M dt \\ &= \frac{2}{\sqrt{3\eta_0}c}\int_{-\infty}^{\infty}\left\{\eta + \frac{3}{4}\eta^2 + \frac{1}{6}\eta_{xx}\right\} d\mathcal{A} \\ &= \frac{2}{\sqrt{3\eta_0}c}\eta_0\left\{\tanh(\mathcal{A}) + \frac{\eta_0}{4}\left[3\tanh(\mathcal{A}) - \tanh^3(\mathcal{A})\right]\right\}_{-\infty}^{\infty}. \end{aligned}$$

The value of this integral is $\frac{4\sqrt{\eta_0}}{\sqrt{3}}$. Comparing this value to the expression found using the approximation (3.6), we see that

$$\frac{4\sqrt{\eta_0}}{\sqrt{3}} - \frac{4\sqrt{\eta_0}}{\sqrt{3}}\frac{1-\frac{\eta_0}{6}}{1+\frac{\eta_0}{2}} = \frac{8}{3\sqrt{3}}\eta_0^{3/2} + \mathcal{O}(\eta_0^{5/2}).$$

Thus we note that the mass flux due to evaluating the differential equation is somewhat larger, and the difference between the two is of order less than 2. Note however that the formula for the mass flux found from the particle paths above was due to the further approximation (3.5), and comparison with the Runge–Kutta method showed that the horizontal displacement of a particle was underestimated. Fig. 5 suggests that the mass flux computed using the Runge–Kutta method is closer to the value $Q = \frac{4\sqrt{\eta_0}}{\sqrt{3}}$, and is therefore more accurate than the value computed using the formula (3.7). The total mass flux can also be computed by simply evaluating the integral $\int_{-\infty}^{\infty}\eta\, dx$, where η is the solitary wave given by (3.1). This approach was used in [27], and it also gives the correct value $\frac{4\sqrt{\eta_0}}{\sqrt{3}}$.

4. Particle paths in periodic waves

Attention will now be turned to particle paths in the fluid flow due to the propagation of periodic traveling waves at the surface. In the KdV approximation, periodic wavetrains are described by exact solutions given in terms of the so-called cnoidal functions [28]. Indeed, it is well known that periodic solutions of (2.10) are given by

$$\eta = f_2 + (f_1 - f_2)\mathrm{cn}^2(\mathcal{B}), \tag{4.1}$$

where the solution is defined by the three constants f_1, f_2 and f_3 which are arranged in the order $f_3 < f_2 < f_1$. In Eq. (4.1), the argument is $\mathcal{B}(x,t) = \frac{\sqrt{3}}{2}(f_1 - f_3)^{1/2}(x - ct)$, cn is one of the Jacobian elliptic functions defined by the incomplete elliptic integral of the first kind [29], and the modulus of cn is given by $m = (f_1 - f_2)/(f_1 - f_3)$. The phase speed of the wave is $c = 1 + (f_1 + f_2 + f_3)/2$, and the wavelength is given by $\lambda = \frac{4}{\sqrt{3}}K(m)\frac{1}{\sqrt{f_1 - f_3}}$, where $K(m)$ is the complete elliptic integral of the first kind. The particle motion is described by the differential equations (3.4) which may be rewritten with the help

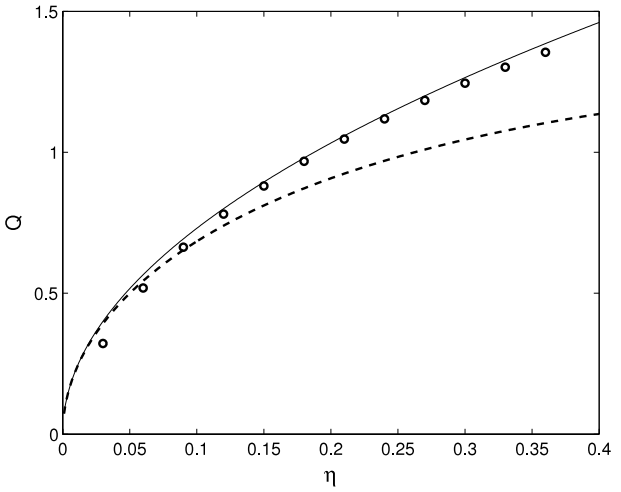

Fig. 5. A comparison of the values of total mass flux. The dashed line shows the formula (3.7). The solid line shows the formula $Q = \frac{4\sqrt{\eta_0}}{\sqrt{3}}$. The circles indicate the mass flux computed from the numerical solution of the particle paths with the Runge–Kutta method, and taking the average over the depth of the fluid.

of (2.7) and (2.8) as

$$\frac{\partial \xi}{\partial t} = w^\theta + \frac{1}{2}(\theta^2 - \zeta^2) w^\theta_{xx}, \qquad \frac{\partial \zeta}{\partial t} = -\zeta\, w^\theta_x. \tag{4.2}$$

Using the relation (2.11), the horizontal velocity may be written in terms of the Jacobian elliptic functions cn, sn and dn as

$$\begin{aligned} w^\theta &= f_2 - \frac{f_2^2}{4} + (f_1 - f_2)\left(1 - \frac{f_2}{2}\right)\mathrm{cn}^2(\mathcal{B}) - \frac{(f_1 - f_2)^2}{4}\mathrm{cn}^4(\mathcal{B}) \\ &\quad - \frac{3}{2}(f_1 - f_3)(f_1 - f_2)\left(\frac{1}{3} - \frac{\theta^2}{2}\right)\left\{-\mathrm{sn}^2(\mathcal{B})\,\mathrm{dn}^2(\mathcal{B}) + \mathrm{cn}^2(\mathcal{B})\,\mathrm{dn}^2(\mathcal{B}) - m\mathrm{cn}^2(\mathcal{B})\,\mathrm{sn}^2(\mathcal{B})\right\}. \end{aligned}$$

The derivatives are given by

$$\begin{aligned} w^\theta_x &= \frac{\sqrt{3}}{2}(f_1 - f_3)^{1/2}\mathrm{cn}(\mathcal{B})\mathrm{sn}(\mathcal{B})\mathrm{dn}(\mathcal{B})\left\{ - (f_1 - f_2)(2 - f_2) + (f_1 - f_2)^2\mathrm{cn}^2(\mathcal{B}) \right. \\ &\quad \left. + \ 6(f_1 - f_3)(f_1 - f_2)\left(\frac{1}{3} - \frac{\theta^2}{2}\right)(\mathrm{dn}^2(\mathcal{B}) + m\mathrm{cn}^2(\mathcal{B}) - m\mathrm{sn}^2(\mathcal{B}))\right\}, \end{aligned}$$

and

$$\begin{aligned} w^\theta_{xx} &= \frac{3}{4}(f_1 - f_3)\left\{ - (f_1 - f_2)(2 - f_2)(-\mathrm{sn}^2(\mathcal{B})\,\mathrm{dn}^2(\mathcal{B}) + \mathrm{cn}^2(\mathcal{B})\,\mathrm{dn}^2(\mathcal{B}) \right. \\ &\quad - m\,\mathrm{cn}^2(\mathcal{B})\,\mathrm{sn}^2(\mathcal{B})) + (f_1 - f_2)^2(-3\mathrm{cn}^2(\mathcal{B})\,\mathrm{sn}^2(\mathcal{B})\,\mathrm{dn}^2(\mathcal{B}) + \mathrm{cn}^4(\mathcal{B})\,\mathrm{dn}^2(\mathcal{B}) \\ &\quad - m\,\mathrm{cn}^4(\mathcal{B})\,\mathrm{sn}^2(\mathcal{B})) + 6(f_1 - f_3)(f_1 - f_2)\left(\frac{1}{3} - \frac{\theta^2}{2}\right)\left[(-\mathrm{sn}^2(\mathcal{B})\,\mathrm{dn}^2(\mathcal{B})\right. \\ &\quad + \mathrm{cn}^2(\mathcal{B})\,\mathrm{dn}^2(\mathcal{B}) - m\,\mathrm{cn}^2(\mathcal{B})\,\mathrm{sn}^2(\mathcal{B}))(\mathrm{dn}^2(\mathcal{B}) + m\,\mathrm{cn}^2(\mathcal{B}) - m\,\mathrm{sn}^2(\mathcal{B})) \\ &\quad \left. \left. - \ 6m\,\mathrm{cn}^2(\mathcal{B})\,\mathrm{sn}^2(\mathcal{B})\,\mathrm{dn}^2(\mathcal{B})\right]\right\}. \end{aligned}$$

Now as in the case of solitary-wave solutions, the Eqs. (4.2) may be integrated numerically if an initial particle location (ξ_0, ζ_0) is given. On the other hand, since the fluid particles may not be displaced a great deal from their initial position during the passage of a surface wave, the approximation (3.5) may also be used to describe the particle paths in the periodic case. To this end, we use (4.2) with the right-hand side fixed at the initial particle location. Then using the relation (2.11), it is found that the x-component of the particle path is given by

$$\begin{aligned} \bar{\xi} - \xi_0 &= \int_0^t \left\{ w^\theta + \frac{1}{2}(\theta^2 - \zeta_0^2) w^\theta_{xx} \right\} dt' \\ &= \int_0^t \left\{ \eta - \frac{1}{4}\eta^2 + \left(\frac{1}{3} - \frac{\theta^2}{2}\right)\eta^\theta_{xx} \right\} dt' + \frac{1}{2}(\theta^2 - \zeta_0^2)\int_0^t w^\theta_{xx}\, dt', \end{aligned}$$

where the integrands are all evaluated at (ξ_0, t'). Note further that the x-derivatives can be written as t derivatives, so that

$$\bar{\xi} - \xi_0 = \int_0^t \left\{\eta - \frac{1}{4}\eta^2\right\} dt' + \left\{-\frac{1}{c}\left(\frac{1}{3} - \frac{\theta^2}{2}\right)\eta_x - \frac{1}{2c}(\theta^2 - \zeta_0^2)w_x^\theta\right\}_0^t.$$

We define $\mathcal{B}_0(t) = \frac{\sqrt{3}}{2}(f_1 - f_3)^{1/2}(\xi_0 - ct)$, and note that

$$\begin{aligned}\int_0^t \left\{\eta - \frac{1}{4}\eta^2\right\} dt' = \left(f_2 - \frac{f_2^2}{4}\right)t - \frac{(f_1 - f_2)}{\sqrt{3}c(f_1 - f_3)^{1/2}}(2 - f_2)\int_{\mathcal{B}_0(0)}^{\mathcal{B}_0(t)} \mathrm{cn}^2(\mathcal{B})\, d\mathcal{B} \\ + \frac{(f_1 - f_2)^2}{2\sqrt{3}c(f_1 - f_3)^{1/2}}\int_{\mathcal{B}_0(0)}^{\mathcal{B}_0(t)} \mathrm{cn}^4(\mathcal{B})\, d\mathcal{B}.\end{aligned}$$

The last two integrals are given by

$$\int \mathrm{cn}^2(\mathcal{B})d\mathcal{B} = \mathcal{B} - \frac{\mathcal{B}}{m} + \frac{E(\mathrm{am}(\mathcal{B}), m)}{m}, \tag{4.3}$$

and

$$\begin{aligned}\int \mathrm{cn}^4(\mathcal{B})d\mathcal{B} = \left(2 - \frac{2}{m}\right)\int \mathrm{cn}^2(\mathcal{B})d\mathcal{B} - \frac{\mathcal{B}}{m^2}\left(\frac{4}{3} - \frac{7}{3}m + m^2\right) \\ + \frac{2}{3}\frac{2 - m}{m^2}E(\mathrm{am}(\mathcal{B}), m) + \frac{1}{3m}\mathrm{cn}(\mathcal{B})\mathrm{sn}(\mathcal{B})\mathrm{dn}(\mathcal{B}).\end{aligned}$$

Here $E(\cdot, m)$ denotes the incomplete elliptic integral of the second kind and $\mathrm{am}(\cdot, m)$ is the Jacobi amplitude function [29]. The z-component of the particle location is treated in a similar way, and substituting the expressions found above, the particle paths are given by the parametric curve

$$\begin{aligned}\bar{\xi}(t) - X_0 = \left(f_2 - \frac{f_2^2}{4}\right)t - \frac{(f_1 - f_2)}{\sqrt{3}c(f_1 - f_3)^{1/2}}(2 - f_2)\left\{\mathcal{B}_0 - \frac{\mathcal{B}_0}{m} + \frac{E(\mathrm{am}(\mathcal{B}_0), m)}{m}\right\} \\ + \frac{(f_1 - f_2)^2}{2\sqrt{3}c(f_1 - f_3)^{1/2}}\left\{\left(1 - \frac{5}{3m} + \frac{2}{3m^2}\right)\mathcal{B}_0 + \frac{2(2m - 1)}{3m^2}E(\mathrm{am}(\mathcal{B}_0), m)\right. \\ \left. + \frac{1}{3m}\mathrm{cn}(\mathcal{B}_0)\mathrm{sn}(\mathcal{B}_0)\mathrm{dn}(\mathcal{B}_0)\right\} + \frac{\sqrt{3}}{c}(f_1 - f_3)^{1/2}(f_1 - f_2)\mathrm{cn}(\mathcal{B}_0)\mathrm{sn}(\mathcal{B}_0)\mathrm{dn}(\mathcal{B}_0) \\ \times \left\{\frac{1}{3} - \frac{\zeta_0^2}{2} + \frac{1}{4}(\theta^2 - \zeta_0^2)\left[-f_2 + (f_1 - f_2)\mathrm{cn}^2(\mathcal{B}_0)\right.\right. \\ \left.\left. + 6(f_1 - f_3)\left(\frac{1}{3} - \frac{\theta^2}{2}\right)(\mathrm{dn}^2(\mathcal{B}_0) + m\,\mathrm{cn}^2(\mathcal{B}_0) - m\,\mathrm{sn}^2(\mathcal{B}_0))\right]\right\}\end{aligned}$$

and

$$\begin{aligned}\bar{\zeta}(t) - Z_0 = \frac{\zeta_0}{c}\left\{f_2 + \frac{f_2^2}{4} - (f_1 - f_2)\left(1 - \frac{f_2}{2}\right)\mathrm{cn}^2(\mathcal{B}_0) - \frac{(f_1 - f_2)^2}{4}\mathrm{cn}^4(\mathcal{B}_0)\right. \\ + \frac{3}{2}(f_1 - f_3)(f_1 - f_2)\left(\frac{1}{3} - \frac{\theta^2}{2}\right)[\mathrm{sn}^2(\mathcal{B}_0)\,\mathrm{dn}^2(\mathcal{B}_0) \\ \left. - \mathrm{cn}^2(\mathcal{B}_0)\,\mathrm{dn}^2(\mathcal{B}_0) + m\mathrm{cn}^2(\mathcal{B}_0)\,\mathrm{sn}^2(\mathcal{B}_0)]\right\}.\end{aligned}$$

As before, the constants X_0 and Z_0 denote the difference between the initial particle locations and the expressions of the right-hand sides when evaluated at $t = 0$ (i.e. at $\mathcal{B}_0(0) = \frac{\sqrt{3}}{2}(f_1 - f_3)^{1/2}\xi_0$). Although these expressions can be programmed easily, their length makes them somewhat impractical. Moreover, these approximations suffer from the same problem as the approximate particle paths (3.6) associated to solitary waves, namely that the horizontal excursion is underestimated. A more satisfactory approach is the direct integration of the differential equations (4.2) by a high-order numerical method, in the same way as (3.4) was solved in the previous section. Of course, here, the expressions for w and its derivatives given above must be used.

Some examples of particle paths will now be presented. We first consider periodic traveling waves in the configuration where the trough of the wave coincides with the undisturbed fluid surface. In this case, the cnoidal wave resembles a train of solitary waves, and if the wavelength is large, it approximates the solitary wave. In Fig. 6, particle paths (ξ, ζ) are shown for one cycle using the Runge–Kutta method. It is evident that the particle paths look similar to those below a solitary wave.

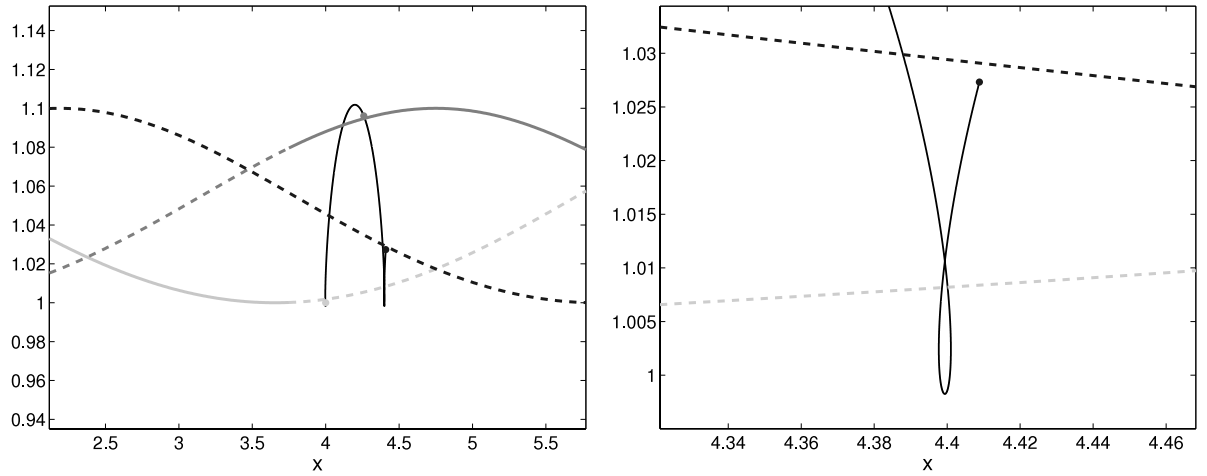

Fig. 6. A periodic wave with wavelength 7.3108, period 7.6956 and phase speed $c = 0.95$ is shown at $t = 0$ (light-gray), $t = 5$ (dark-gray) and $t = 10$ (black). The solid part of the curve is kept constant, indicating the movement of the surface. The path of a particle initially located at $(x, z) = (4, 1)$ is shown. The right panel shows a close-up of the lower turning point.

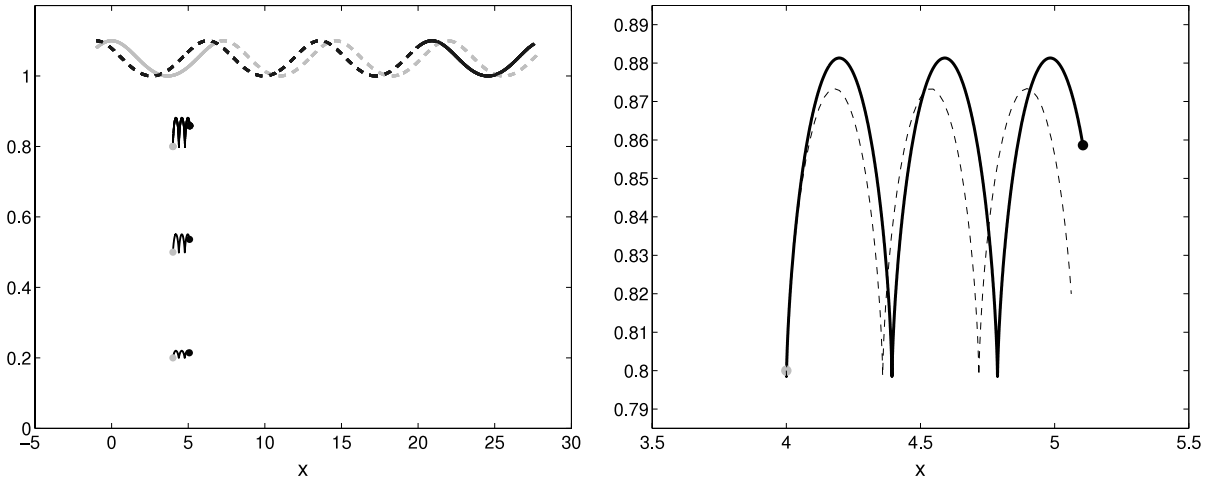

Fig. 7. A periodic wave with wavelength 7.3108, period 7.6956 and phase speed $c = 0.95$ is shown at $t = 0$ (light-gray) and $t = 22$ (black). The solid part of the curve is kept constant, indicating the movement of the surface. The paths of particles initially located at (4, 0.8), (4, 0.5) and (5, 0.2) are shown. In the right panel, a closeup of the path of a particle located initially at (4, 0.8) is shown, and compared to the approximate trajectory $(\bar{\xi}, \bar{\zeta})$, which is shown as a dashed curve.

The periodicity however is still important as the closeup shows. There, we see that the particle actually completes a small elliptic cycle before it turns up again, and rides into the next wave.

In Fig. 7, a train of cnoidal waves is shown, and a comparison between the numerical integration of (4.2) and the asymptotic approximation $(\bar{\xi}, \bar{\zeta})$ is made. The particles closer to the bottom have smaller vertical speed, and smaller total vertical excursion. It is also visible that the asymptotic approximation $(\bar{\xi}, \bar{\zeta})$ yields a shorter particle path. This is similar to the results concerning particle paths beneath solitary waves in the previous section.

If the crest and trough of the cnoidal wave are taken to be such that the mean level is zero, then the particle paths are nearly closed. For small amplitudes, these waves can be approximated by the sinusoidal waves which are the hallmark of the linearized water-wave problem. Fig. 8 shows some particle paths below a periodic cnoidal wave with amplitude 0.06, and wavelength 2π. The crest of the wave is centered at $x = 0$, and the particles are initially located at $x = \pi/2$, and $z = 0.1, 0.2 \cdots 1$. The dashed curves indicate particle paths given by $(\bar{\xi}, \bar{\zeta})$. In the right panel of Fig. 8, it can be seen that when the approximation $(\bar{\xi}, \bar{\zeta})$ is used, then the particle paths are nearly closed. However, there is a slight defect, which can already by anticipated by observing that the horizontal excursion of the particles is too short both in the case of solitary waves (Fig. 4), and in the previous case shown in Figs. 6 and 7. Thus in this case, as opposed to the linear water-wave problem, the particle paths are not completely closed if the approximation (3.5) for $(\bar{\xi}, \bar{\zeta})$ is made. In column 4 of Tables 1 and 2, the backward drift due to this defect is tabulated as a function of the wave amplitude at the surface. Note that the defect does not depend on the initial depth of the particle, a fact which can be understood by examining the formula for $(\bar{\xi}, \bar{\zeta})$, and

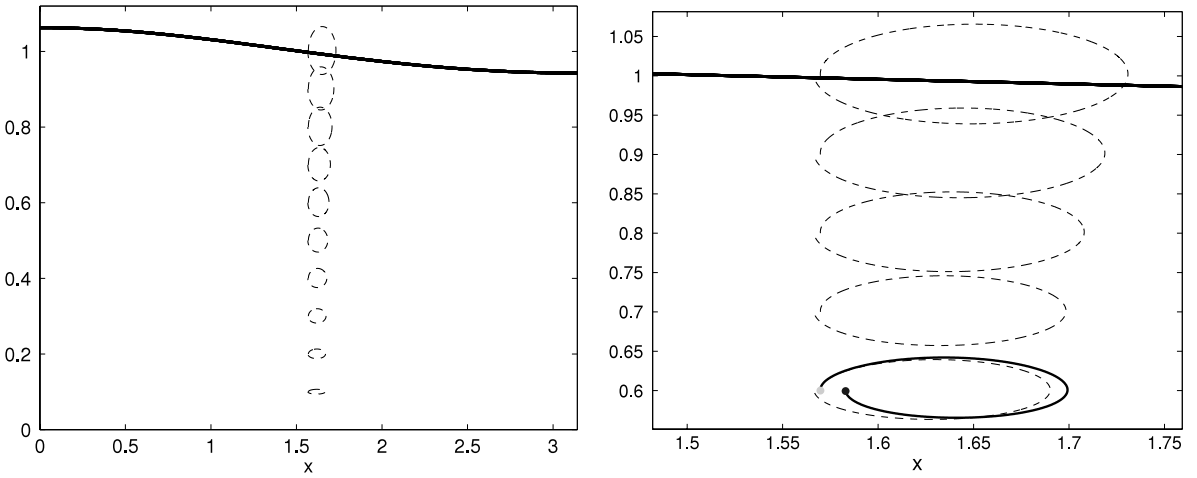

Fig. 8. This figure shows the full cycle of a periodic traveling wave with amplitude 0.06 and wavelength 2π. Paths of particles initially located at $x = \pi/2$ and a variety of initial depths are shown. The dashed curves are obtained with the formula for $(\bar{\xi}, \bar{\zeta})$. The trajectory indicated by a solid curve in the right panel is obtained by numerical approximation.

Table 1
The first three columns of this table show the amplitude, time period, and phase speed of a periodic traveling-wave solution of the KdV equation. The wavelength is $\lambda = 2\pi$. The fourth column shows the defect in the particle paths after one period if the approximation $(\bar{\xi}, \bar{\zeta})$ is used. The fifth column shows the actual forward drift for a particle located initially at a depth of $\zeta_0 = 0.5$, computed using equation (4.4). The sixth column shows the Stokes drift of a linear wave of the same wavelength and amplitude, and for a particle located at the same position. The phase speed of the linear wave is 0.8727.

Amplitude	Period	Phase speed	Defect	Forward drift	Stokes drift
0.06	7.5214	0.8354	−0.0004	0.0016	0.0018
0.12	7.4676	0.8414	−0.0018	0.0073	0.0070
0.18	7.3814	0.8512	−0.0040	0.0186	0.0158
0.24	7.2672	0.8646	−0.0070	0.0384	0.0281
0.30	7.1301	0.8812	−0.0109	0.0691	0.0439

Table 2
The first three columns of this table show the amplitude, time period, and phase speed of a periodic traveling-wave solution of the KdV equation. The wavelength is $\lambda = 5\pi$. The fourth column shows the defect in the particle paths after one period if the approximation $(\bar{\xi}, \bar{\zeta})$ is used. The fifth column shows the actual forward drift for a particle located initially at a depth of $\zeta_0 = 0.8$, computed using Eq. (4.4). The sixth column shows the Stokes drift of a linear wave of the same wavelength and amplitude, and for a particle located at the same position. The phase speed of the linear wave is 0.9746.

Amplitude	Period	Phase speed	Defect	Forward drift	Stokes drift
0.06	15.9517	0.9850	−0.0004	0.0017	0.0020
0.12	15.5134	1.0127	−0.0016	0.0072	0.0081
0.18	14.9893	1.0480	−0.0029	0.0176	0.0181
0.24	14.4461	1.0874	−0.0055	0.0342	0.0323
0.30	13.9093	1.1293	−0.0081	0.0590	0.0504

observing that the part which depends on ζ_0 is periodic. In the linear water-wave problem, it is customary to approximate the integrands at the central point of the particle path, but here we used the initial point in order to approximate the integrals involved in evaluating the particle paths. Experimentation with different fixed locations did not yield a great variation in the particle paths in the case of the cnoidal traveling waves. In particular, it was not possible to find closed curves for $(\bar{\xi}, \bar{\zeta})$.

In the right panel of Fig. 8, the solid curve indicates the numerical approximation of a particle path starting at $(x, z) = (\pi/2, 0.6)$. It is clear from this picture that if the numerical solution is used, then the particles experience a forward drift, similar to the well known Stokes drift in the linear approximation. In column 5 of Tables 1 and 2, the forward drift during one period is computed by using the Runge–Kutta method, and for comparison, the Stokes drift as computed by a second-order Taylor expansion for *linear* periodic water waves is shown in column 6. In the present non-dimensional case, the formula is given by

$$\bar{u}_L = a^2 \omega k \frac{\cosh 2kz}{2 \sinh^2 k}, \tag{4.4}$$

where $\omega = \sqrt{k \tanh k}$, and z is measured from the horizontal bottom.

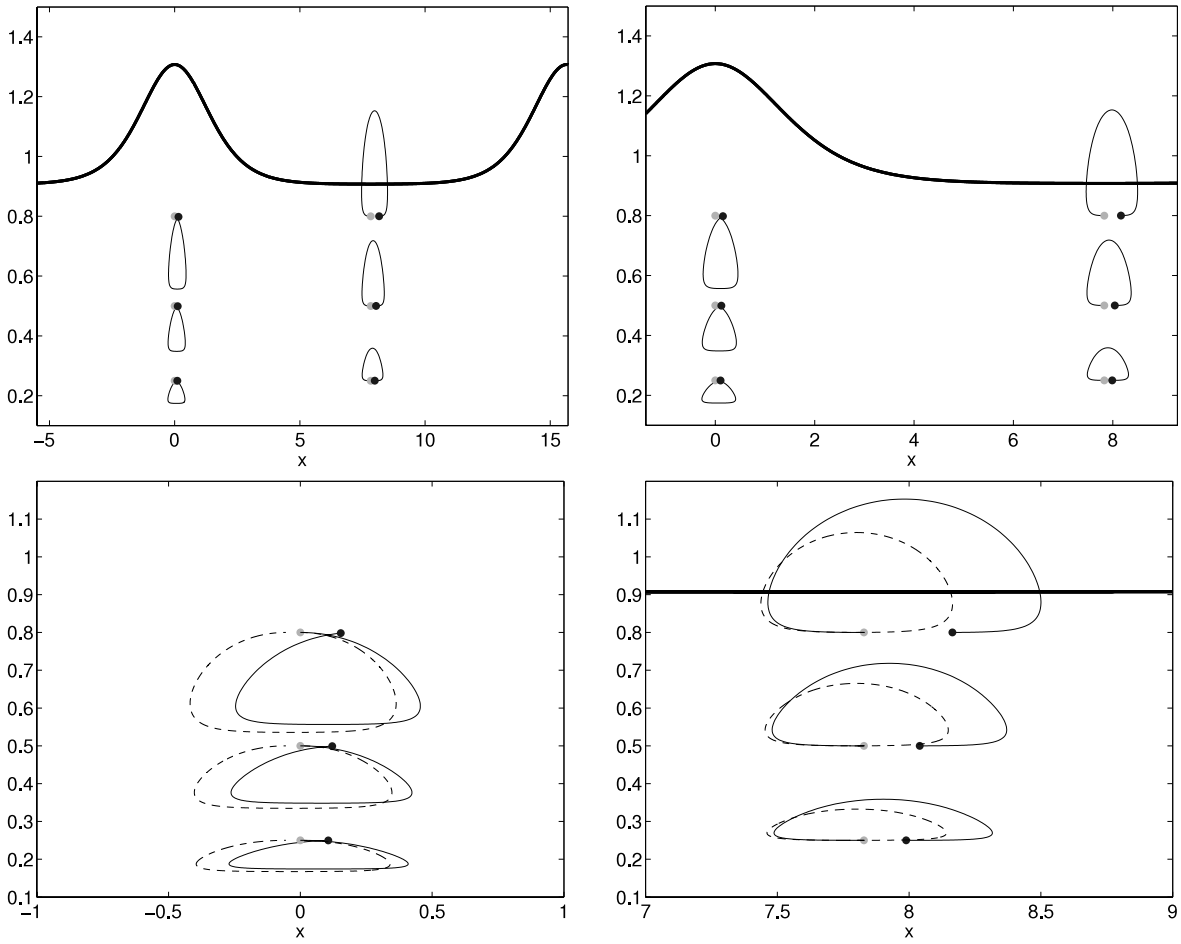

Fig. 9. This figure shows a wave with wavelength 15.659. The upper left panel shows 1.5 wavelengths of the surface wave, and a number of particle trajectories (ξ, ζ) with initial x-coordinates $x = 0$ and $x = 7.829$, and initial z-coordinates $z = 0.25$, $z = 0.5$ and $z = 0.8$. A close-up of particle paths starting below the crest and below the trough of the surface wave is shown in the upper right panel. The lower panels show even closer pictures of the particle paths, and comparisons to the approximate particle paths $(\bar{\xi}, \bar{\zeta})$ which are displayed as dashes curves.

Table 2 shows a comparison of the defect in the particle path given by $(\bar{\xi}, \bar{\zeta})$, the forward drift experienced by the numerical approximation of (ξ, ζ), and the Stokes drift for a linear periodic wave of the same amplitude. Here, the wavelength of the cnoidal traveling wave is 5π. We note that the forward drift in the KdV approximation agrees well with the Stokes drift, for small amplitudes, but becomes larger than the Stokes drift with increasing amplitude. Although not shown here, it appears that the forward drift depends more strongly on the initial position of the particle in the KdV approximation than in the linear approximation. Further examples of the forward drift of a particle during one period are shown in Fig. 9. The evolution of a particle in the surface during several cycles of a periodic wave is shown in Fig. 10.

5. Particle paths in soliton interactions

As mentioned in the introduction, the KdV equation features exact two-soliton solutions given in closed form [30]. With such a formula in hand, one may then use (2.7)–(2.9) to find the velocity field associated to the interaction of two solitary waves on the surface. The two-soliton solution of the KdV equation is given by

$$\eta(x,t) = 32\,\frac{k_1^2E_1 + k_2^2E_2 + 2(k_1-k_2)^2E_1E_2 + A(k_1^2E_2 + k_2^2E_1)E_1E_2}{(1 + E_1 + E_2 + AE_1E_2)^2}. \tag{5.1}$$

Here k_i, $i = 1, 2$ are the wave numbers, x_{0i}, $i = 1, 2$ are arbitrary phases, A is given by $A = (k_1 - k_2)^2/(k_1 + k_2)^2$ and

$$E_i = \exp\{2\sqrt{6}k_i(x - x_{0i} - (1 + 4k_i^2)t)\}, \quad i = 1, 2.$$

Note that this formula reduces correctly to the one-soliton solution if k_1 or k_2 are taken as zero. For example if $k_2 = 0$, (5.1) takes the form

$$\eta(x,t) = 8k_1^2\,\mathrm{sech}^2\left\{2\sqrt{6}k_1(x - x_{01} - (1 + 4k_1^2)t)\right\}.$$

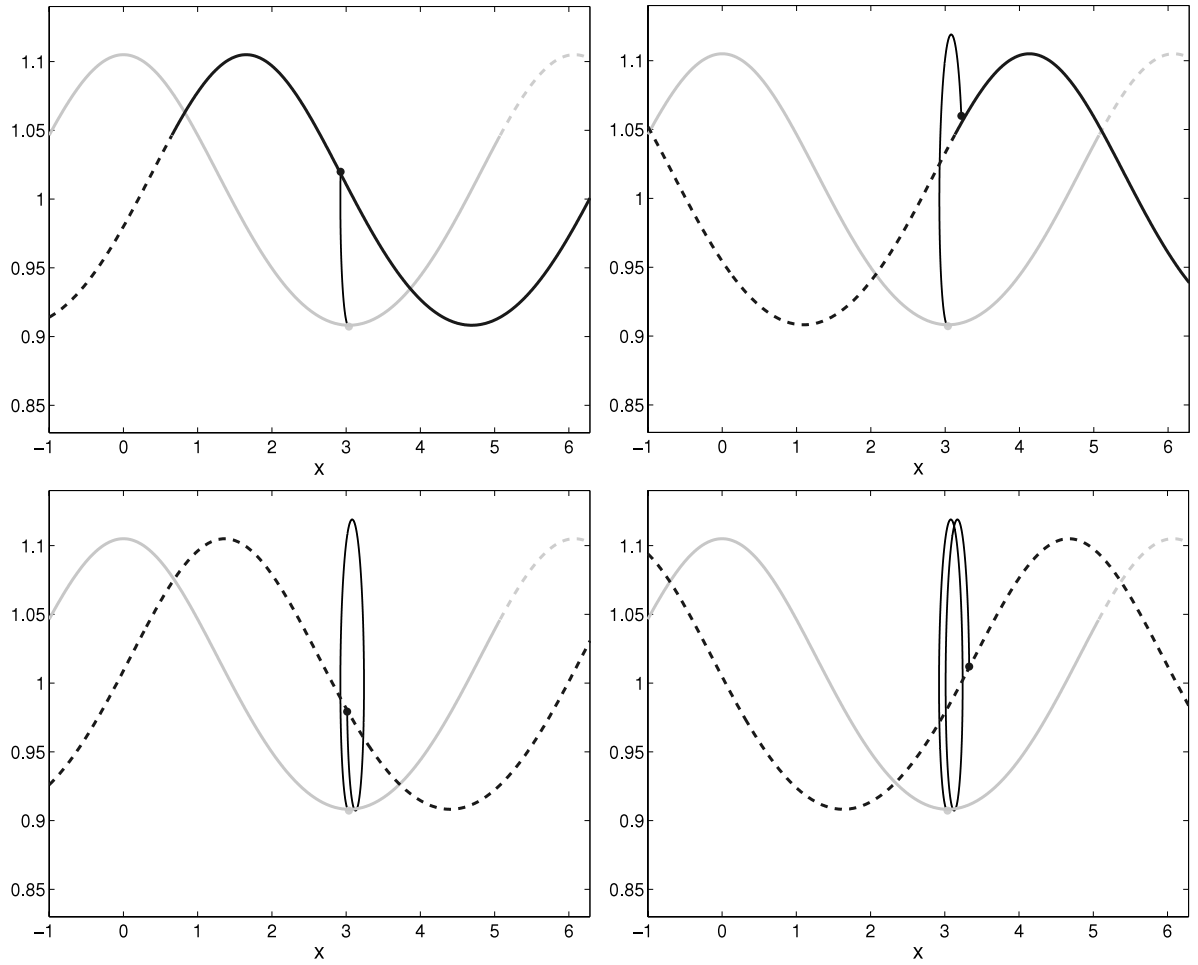

Fig. 10. A periodic wave with wavelength 6.08, period 7.35 and phase speed $c = 0.827$ and mean zero is shown at $t = 0$ (light-gray) and $t = 2$, $t = 5$, $t = 9$ and $t = 13$ (black). The solid part of the curve is kept constant, indicating the movement of the surface. The path of a particle initially located at (3.04, 0.907) is shown.

Using (2.11) in the expressions of horizontal and vertical velocities, given by (2.7) and (2.8), respectively, one can write

$$u(x,z,t) = \eta - \frac{1}{4}\eta^2 + \frac{1}{3}\eta_{xx} - \frac{1}{2}z^2\eta_{xx} + \frac{1}{2}(\theta^2 - z^2)\left[-\frac{1}{2}(\eta_x^2 + \eta\eta_{xx}) + \left(-\frac{\theta^2}{2} + \frac{1}{3}\right)\eta_{xxxx}\right],$$

and

$$v(x,z,t) = -z\left[\eta_x - \frac{1}{2}\eta\eta_x + \left(\frac{1}{3} - \frac{\theta^2}{2}\right)\eta_{xxx}\right].$$

It appears that evaluation of the velocity field involves finding the spatial derivatives of η up to order 4. This task can be carried out efficiently with the software package *Maple* for instance. Since the formulas are rather expansive, they have been tabulated in the Appendix for the reader's convenience.

Once the horizontal and vertical velocities are evaluated, they can be inserted into the differential equations (3.4), and these can be integrated numerically using the four-stage Runge–Kutta scheme. As in the previous sections, this strategy yields approximations to the parametric curves traced out by particles in the fluid. An example is shown in Figs. 11 and 12. There we have chosen $k_1 = 0.1$ and $k_1 = 0.24$, corresponding to solitary waves with amplitudes 0.08 and 0.46, respectively. Fig. 11 shows the trajectory during a soliton-interaction of a particle located close to the free surface. Fig. 12 shows particle paths for a number of particles located at a greater depth. Finally, Fig. 13 shows a comparison of particle paths due to the interaction of solitary waves, and paths due to the individual solitary waves.

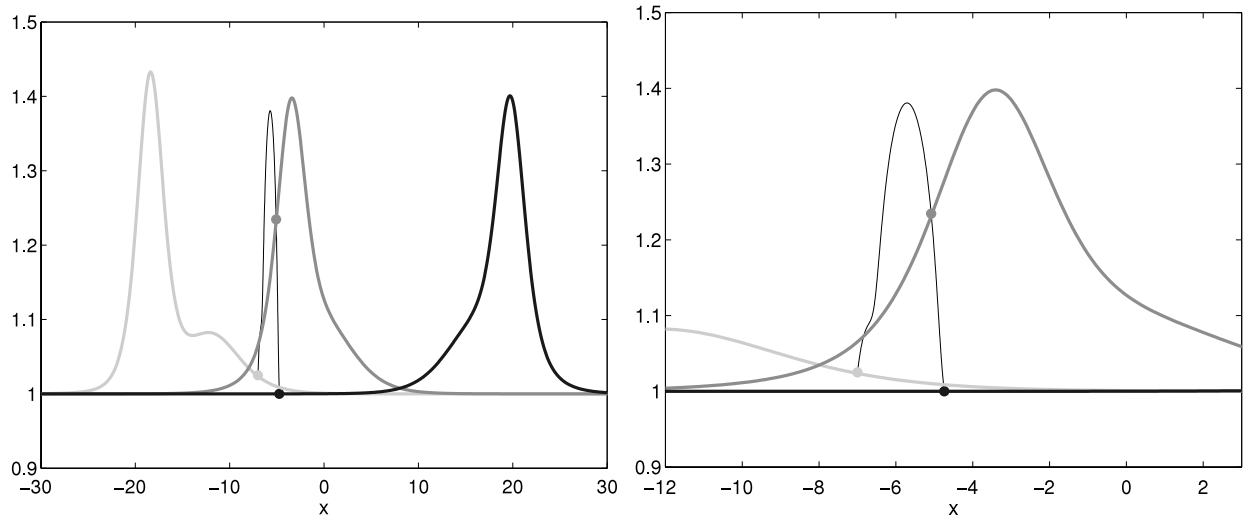

Fig. 11. This figure shows the interaction of two solitary waves with amplitudes 0.08 and 0.46. The wave is shown at $t = 0$ (light-gray), $t = 6$ (dark-gray) and $t = 15$ (black). The trajectory of a fluid particle located close to the free surface is by the thin black curve, and the particle positions at the three times where the wave is shown is indicated by dots.

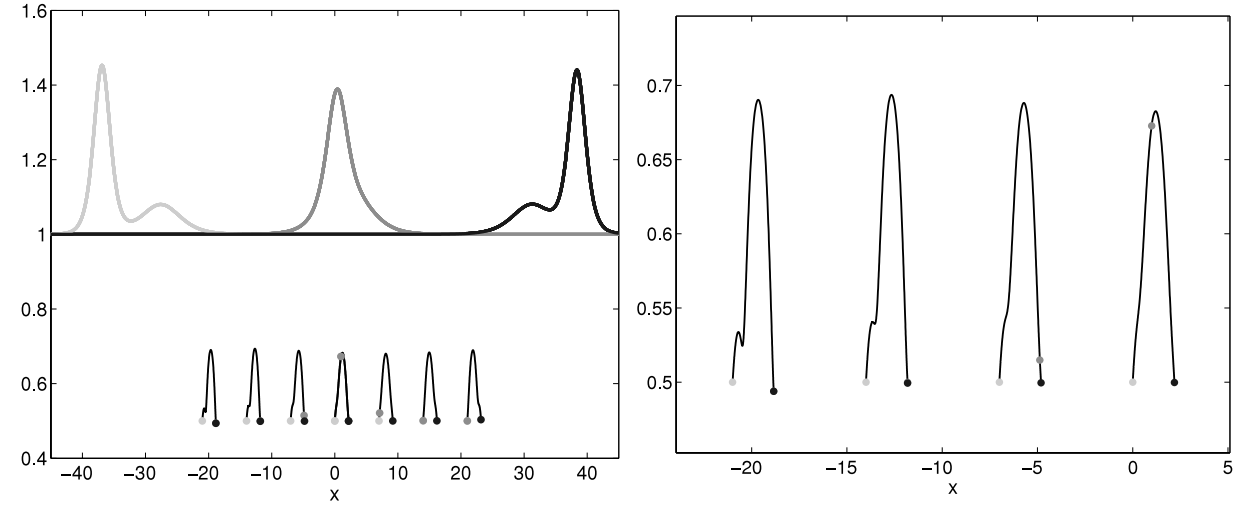

Fig. 12. This figure shows the interaction of two solitary waves with amplitudes 0.08 and 0.46. Several particle paths are shown for particles originally located at depth $z = 0.5$. The initial x-coordinates are $x = -21$, $x = -14$, $x = -7$, $x = 0$, $x = 7$, $x = 14$, and $x = 21$.

6. Conclusion

In this article, it has been shown that the KdV approximation may be used to describe the motion of particles in the fluid column below a surface wave. While solutions of the KdV equation represent wave patterns at the surface of the fluid, the derivation of the KdV equation shows that it is possible to deduce expressions for the velocity field of the fluid below the surface. The particle paths are described by two coupled ordinary differential equations which are defined in terms of the velocity field associated to a surface wave.

The solutions can be approximated in two ways. First, the particle location is assumed fixed on the right-hand side of each equation, and this method yields an exact formula which is valid asymptotically in the limit of small amplitude. This technique hails from the study of the linear water-wave problem where it can be used to show that particle paths in linear water waves are close to ellipses (however, as shown in [9,11], particle paths due to periodic surface waves are never closed, not even in the linear approximation). The second method of approximation is the direct numerical integration of the ordinary differential equations governing the particle motion. Also here, the KdV approximation is crucial in providing explicit formulas which can then be integrated numerically.

A number of tests have been performed on the resulting approximations of the particle paths. We have computed the mass flux due to a surface solitary wave, and the forward drift due to a periodic cnoidal surface wave. In all cases, it

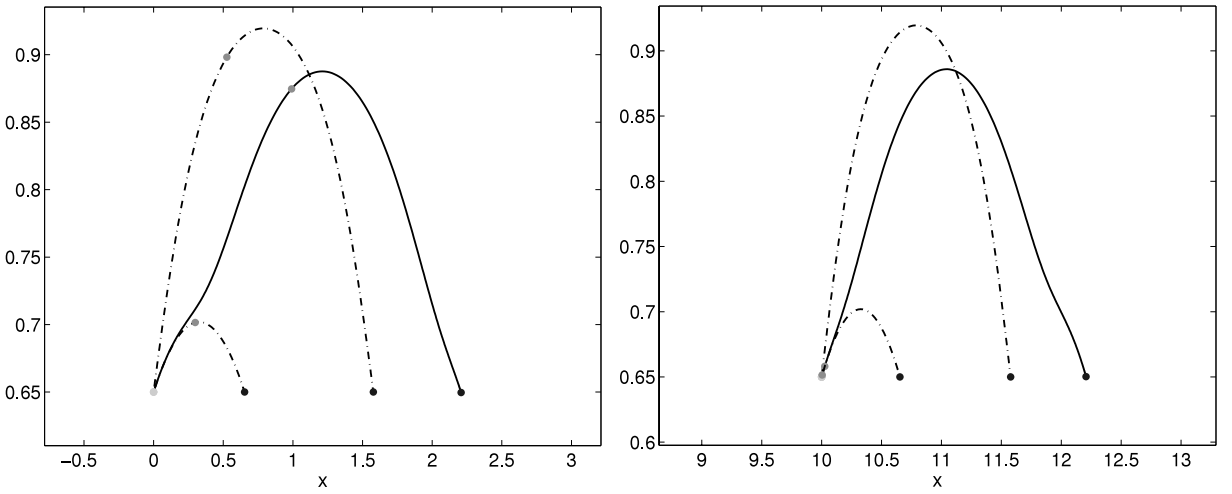

Fig. 13. This figure shows particle paths associated with the interaction of two solitary waves with amplitudes 0.08 and 0.46. The particles are originally located at $z = 0.65$, $x = 0$ (left panel), and $x = 10$ (right panel). The dashed–dotted curves represent the corresponding particle paths associated to the passage of a single solitary wave.

appears that the numerical integration of the equations gives more favorable results. However, just as in the linear case, the asymptotic small-amplitude approximation is also useful because it is given in exact form.

Finally, it should be mentioned that the velocity field (2.7), (2.8) constructed from the derivation of the KdV equation is irrotational and incompressible up to the same order as the KdV equation is valid. This can be seen immediately from the discussion surrounding the derivation of the equation in [6].

Acknowledgments

The first author was visiting the University of Bergen during the preparation of this manuscript, and acknowledges the support of the Research Council of Norway through the YGGDRASIL program. The second author acknowledges support of the Research Council of Norway through grant no. 213474/F20.

Appendix

The first four spatial derivatives of $\eta(x, t)$ given by (5.1) are tabulated.

$$
\begin{aligned}
\eta_x &= \frac{1}{(1+E_2+E_1+AE_1E_2)^2}\{2k^3\sqrt{6}E_1 + 2l^3\sqrt{6}E_2 + 4\,(k-l)^2\sqrt{6}kE_1E_2 \\
&\quad + 4\,(k-l)^2E_1\sqrt{6}lE_2 + A(2l^2\sqrt{6}kE_1 + 2k^2\sqrt{6}lE_2)E_1E_2 \\
&\quad + 2A(l^2E_1 + k^2E_2)\sqrt{6}kE_1E_2 + 2A(l^2E_1 + k^2E_2)E_1\sqrt{6}lE_2\} \\
&\quad - \frac{2}{(1+E_2+E_1+AE_1E_2)^3}\{[k^2E_1 + l^2E_2 + 2\,(k-l)^2E_1E_2 \\
&\quad + A(l^2E_1 + k^2E_2)E_1E_2][2\sqrt{6}lE_2 + 2\sqrt{6}kE_1 + 2A\sqrt{6}kE_1E_2 + 2AE_1\sqrt{6}lE_2]\} \\
\eta_{xx} &= \frac{1}{(1+E_2+E_1+AE_1E_2)^2}(24k^4E_1 + 24l^4E_2 + 48\,(k-l)^2k^2E_1E_2 \\
&\quad + 96\,(k-l)^2klE_1E_2 + 48\,(k-l)^2E_1l^2E_2 + A(24l^2k^2E_1 + 24k^2l^2E_2)E_1E_2 \\
&\quad + 4A(2l^2\sqrt{6}kE_1 + 2k^2\sqrt{6}lE_2)\sqrt{6}kE_1E_2 \\
&\quad + 4A(2l^2\sqrt{6}kE_1 + 2k^2\sqrt{6}lE_2)E_1\sqrt{6}lE_2 + 24A(l^2E_1 \\
&\quad + k^2E_2)k^2E_1E_2 + 48A(l^2E_1 + k^2E_2)klE_1E_2 + 24A(l^2E_1 + k^2E_2)E_1l^2E_2) \\
&\quad - \frac{4}{(1+E_2+E_1+AE_1E_2)^3}(2k^3\sqrt{6}E_1 + 2l^2\sqrt{6}lE_2 + 4\,(k-l)^2\sqrt{6}kE_1E_2 \\
&\quad + 4\,(k-l)^2E_1\sqrt{6}lE_2 + A(2l^2\sqrt{6}kE_1 + 2k^2\sqrt{6}lE_2)E_1E_2 \\
&\quad + 2A(l^2E_1 + k^2E_2)\sqrt{6}kE_1E_2 + 2A(l^2E_1 + k^2E_2)E_1\sqrt{6}lE_2)(2\sqrt{6}lE_2
\end{aligned}
$$

$$
\begin{aligned}
&+2\sqrt{6}kE_1+2A\sqrt{6}kE_1E_2+2AE_1\sqrt{6}lE_2)\\
&+\frac{6}{(1+E_2+E_1+AE_1E_2)^4}(k^2E_1+l^2E_2+2(k-l)^2E_1E_2\\
&+A(l^2E_1+k^2E_2)E_1E_2)(2\sqrt{6}lE_2+2\sqrt{6}kE_1+2A\sqrt{6}kE_1E_2+2AE_1\sqrt{6}lE_2)^2\\
&-\frac{2}{(1+E_2+E_1+AE_1E_2)^3}(k^2E_1+l^2E_2+2(k-l)^2E_1E_2\\
&+A(l^2E_1+k^2E_2)E_1E_2)(24l^2E_2+24k^2E_1+24Ak^2E_1E_2\\
&+48AklE_1E_2+24AE_1l^2E_2)\\
\eta_{xxx} &= \frac{1}{(1+E_2+E_1+AE_1E_2)^2}(144A(l^2E_1+k^2E_2)k^2E_1\sqrt{6}lE_2\\
&+144A(l^2E_1+k^2E_2)kE_1l^2\sqrt{6}E_2+48k^5\sqrt{6}E_1+48l^5\sqrt{6}E_2\\
&+6A(24l^2k^2E_1+24k^2l^2E_2)\sqrt{6}kE_1E_2+6A(24l^2k^2E_1+24k^2l^2E_2)E_1\sqrt{6}lE_2\\
&+144A(2l^2\sqrt{6}kE_1+2k^2\sqrt{6}lE_2)klE_1E_2+48A(l^2E_1+k^2E_2)k^3\sqrt{6}E_1E_2\\
&+48A(l^2E_1+k^2E_2)E_1l^3\sqrt{6}E_2+96(k-l)^2k^3\sqrt{6}E_1E_2+96(k-l)^2E_1l^3\sqrt{6}E_2\\
&+72A(2l^2\sqrt{6}kE_1+2k^2\sqrt{6}lE_2)k^2E_1E_2+72A(2l^2\sqrt{6}kE_1\\
&+2k^2\sqrt{6}lE_2)E_1l^2E_2+288(k-l)^2k^2E_1\sqrt{6}lE_2\\
&+A(48l^2k^3\sqrt{6}E_1+48k^2l^3\sqrt{6}E_2)E_1E_2+288(k-l)^2kE_1l^2\sqrt{6}E_2)\\
&-\frac{6}{(1+E_2+E_1+AE_1E_2)^3}((24k^4E_1+24l^4E_2+48(k-l)^2k^2E_1E_2\\
&+96(k-l)^2klE_1E_2+48(k-l)^2E_1l^2E_2+A(24l^2k^2E_1+24k^2l^2E_2)E_1E_2\\
&+4A(2l^2\sqrt{6}kE_1+2k^2\sqrt{6}lE_2)\sqrt{6}kE_1E_2+4A(2l^2\sqrt{6}kE_1\\
&+2k^2\sqrt{6}lE_2)E_1\sqrt{6}lE_2+24A(l^2E_1+k^2E_2)k^2E_1E_2\\
&+48A(l^2E_1+k^2E_2)klE_1E_2+24A(l^2E_1+k^2E_2)E_1l^2E_2)(2\sqrt{6}lE_2+2\sqrt{6}kE_1\\
&+2A\sqrt{6}kE_1E_2+2AE_1\sqrt{6}lE_2))+\frac{18}{(1+E_2+E_1+AE_1E_2)^4}((2k^3\sqrt{6}E_1\\
&+2l^3\sqrt{6}E_2+4(k-l)^2\sqrt{6}kE_1E_2+4(k-l)^2E_1\sqrt{6}lE_2+A(2l^2\sqrt{6}kE_1\\
&+2k^2\sqrt{6}lE_2)E_1E_2+2A(l^2E_1+k^2E_2)\sqrt{6}kE_1E_2\\
&+2A(l^2E_1+k^2E_2)E_1\sqrt{6}lE_2)(2\sqrt{6}lE_2+2\sqrt{6}kE_1\\
&+2A\sqrt{6}kE_1E_2+2AE_1\sqrt{6}lE_2)^2)\\
&-\frac{6}{(1+E_2+E_1+AE_1E_2)^3}((2k^3\sqrt{6}E_1+2l^3\sqrt{6}E_2+4(k-l)^2\sqrt{6}kE_1E_2\\
&+4(k-l)^2E_1\sqrt{6}lE_2+A(2l^2\sqrt{6}kE_1+2k^2\sqrt{6}lE_2)E_1E_2\\
&+2A(l^2E_1+k^2E_2)\sqrt{6}kE_1E_2+2A(l^2E_1+k^2E_2)E_1\sqrt{6}lE_2)(24l^2E_2\\
&+24k^2E_1+24Ak^2E_1E_2+48AkE_1lE_2+24AE_1l^2E_2))\\
&-\frac{24}{(1+E_2+E_1+AE_1E_2)^5}((k^2E_1+l^2E_2+2(k-l)^2E_1E_2\\
&+A(l^2E_1+k^2E_2)E_1E_2)(2\sqrt{6}lE_2+2\sqrt{6}kE_1+2A\sqrt{6}kE_1E_2\\
&+2AE_1\sqrt{6}lE_2)^3)+\frac{18}{(1+E_2+E_1+AE_1E_2)^4}((k^2E_1+l^2E_2\\
&+2(k-l)^2E_1E_2+A(l^2E_1+k^2E_2)E_1E_2)(2\sqrt{6}lE_2+2\sqrt{6}kE_1+2A\sqrt{6}kE_1E_2\\
&+2AE_1\sqrt{6}lE_2)(24l^2E_2+24k^2E_1+24Ak^2E_1E_2+48AkE_1lE_2\\
&+24AE_1l^2E_2))-\frac{2}{(1+E_2+E_1+AE_1E_2)^3}((k^2E_1+l^2E_2+2(k-l)^2E_1E_2\\
&+A(l^2E_1+k^2E_2)E_1E_2)(48l^3\sqrt{6}E_2+48k^3\sqrt{6}E_1+48Ak^3\sqrt{6}E_1E_2\\
&+144Ak^2E_1\sqrt{6}lE_2+144AkE_1l^2\sqrt{6}E_2+48AE_1l^3\sqrt{6}E_2))
\end{aligned}
$$

$$
\begin{aligned}
\eta_{xxxx} = {} & \frac{1}{(1+E_2+E_1+AE_1E_2)^2}(144\,A(24\,l^2k^2E_1+24\,k^2l^2E_2)k^2E_1E_2\\
& +144\,A(24\,l^2k^2E_1+24\,k^2l^2E_2)E_1l^2E_2+576\,A(l^2E_1+k^2E_2)k^4E_1E_2\\
& +576\,A(l^2E_1+k^2E_2)E_1l^4E_2+4608\,(k-l)^2k^3E_1lE_2+4608\,(k-l)^2kE_1l^3E_2\\
& +6912\,(k-l)^2k^2E_1l^2E_2+576\,A(2\,l^2\sqrt{6}kE_1+2\,k^2\sqrt{6}lE_2)k^2E_1\sqrt{6}lE_2\\
& +576\,A(2\,l^2\sqrt{6}kE_1+2\,k^2\sqrt{6}lE_2)kE_1l^2\sqrt{6}E_2+288\,A(24\,l^2k^2E_1\\
& +24\,k^2l^2E_2)kE_1lE_2+8\,A(48\,l^2k^3\sqrt{6}E_1+48\,k^2l^3\sqrt{6}E_2)E_1\sqrt{6}lE_2\\
& +192\,A(2\,l^2\sqrt{6}kE_1+2\,k^2\sqrt{6}lE_2)k^3\sqrt{6}E_1E_2\\
& +192\,A(2\,l^2\sqrt{6}kE_1+2\,k^2\sqrt{6}lE_2)E_1l^3\sqrt{6}E_2+2304\,A(l^2E_1+k^2E_2)kE_1l^3E_2\\
& +3456\,A(l^2E_1+k^2E_2)k^2E_1l^2E_2+8\,A(48\,l^2k^3\sqrt{6}E_1\\
& +48\,k^2l^3\sqrt{6}E_2)\sqrt{6}kE_1E_2+1152\,(k-l)^2k^4E_1E_2\\
& +1152\,(k-l)^2E_1l^4E_2+A(576\,l^2k^4E_1+576\,k^2l^4E_2)E_1E_2\\
& +2304\,A(l^2E_1+k^2E_2)k^3E_1lE_2+576\,k^6E_1+576\,l^6E_2)\\
& -\frac{8}{(1+E_2+E_1+AE_1E_2)^3}((144\,A(l^2E_1+k^2E_2)k^2E_1\sqrt{6}lE_2\\
& +144\,A(l^2E_1+k^2E_2)kE_1l^2\sqrt{6}E_2+48\,k^5\sqrt{6}E_1+48\,l^5\sqrt{6}E_2\\
& +6\,A(24\,l^2k^2E_1+24\,k^2l^2E_2)\sqrt{6}kE_1E_2+6\,A(24\,l^2k^2E_1+24\,k^2l^2E_2)E_1\sqrt{6}lE_2\\
& +144\,A(2\,l^2\sqrt{6}kE_1+2\,k^2\sqrt{6}lE_2)klE_1E_2+48\,A(l^2E_1+k^2E_2)k^3\sqrt{6}E_1E_2\\
& +48\,A(l^2E_1+k^2E_2)E_1l^3\sqrt{6}E_2+96\,(k-l)^2k^3\sqrt{6}E_1E_2+96\,(k-l)^2E_1l^3\sqrt{6}E_2\\
& +72\,A(2\,l^2\sqrt{6}kE_1+2\,k^2\sqrt{6}lE_2)k^2E_1E_2+72\,A(2\,l^2\sqrt{6}kE_1\\
& +2\,k^2\sqrt{6}lE_2)E_1l^2E_2+288\,(k-l)^2k^2E_1\sqrt{6}lE_2+A(48\,l^2k^3\sqrt{6}E_1\\
& +48\,k^2l^3\sqrt{6}E_2)E_1E_2+288\,(k-l)^2kE_1l^2\sqrt{6}E_2)(2\,\sqrt{6}lE_2\\
& +2\,\sqrt{6}kE_1+2\,A\sqrt{6}kE_1E_2+2\,AE_1\sqrt{6}lE_2))\\
& +\frac{36}{(1+E_2+E_1+AE_1E_2)^4}((24\,k^4E_1+24\,l^4E_2+48\,(k-l)^2k^2E_1E_2\\
& +96\,(k-l)^2kE_1lE_2+48\,(k-l)^2E_1l^2E_2+A(24\,l^2k^2E_1+24\,k^2l^2E_2)E_1E_2\\
& +4\,A(2\,l^2\sqrt{6}kE_1+2\,k^2\sqrt{6}lE_2)\sqrt{6}kE_1E_2+4\,A(2\,l^2\sqrt{6}kE_1\\
& +2\,k^2\sqrt{6}lE_2)E_1\sqrt{6}lE_2+24\,A(l^2E_1+k^2E_2)k^2E_1E_2\\
& +48\,A(l^2E_1+k^2E_2)klE_1E_2+24\,A(l^2E_1+k^2E_2)E_1l^2E_2)(2\,\sqrt{6}lE_2+2\,\sqrt{6}kE_1\\
& +2\,A\sqrt{6}kE_1E_2+2\,AE_1\sqrt{6}lE_2)^2)\\
& -\frac{12}{(1+E_2+E_1+AE_1E_2)^3}((24\,k^4E_1+24\,l^4E_2+48\,(k-l)^2k^2E_1E_2\\
& +96\,(k-l)^2kE_1lE_2+48\,(k-l)^2E_1l^2E_2+A(24\,l^2k^2E_1+24\,k^2l^2E_2)E_1E_2\\
& +4\,A(2\,l^2\sqrt{6}kE_1+2\,k^2\sqrt{6}lE_2)\sqrt{6}kE_1E_2+4\,A(2\,l^2\sqrt{6}kE_1\\
& +2\,k^2\sqrt{6}lE_2)E_1\sqrt{6}lE_2+24\,A(l^2E_1+k^2E_2)k^2E_1E_2\\
& +48\,A(l^2E_1+k^2E_2)kE_1lE_2+24\,A(l^2E_1+k^2E_2)E_1l^2E_2)(24\,l^2E_2+24\,k^2E_1\\
& +24\,Ak^2E_1E_2+48\,AkE_1lE_2+24\,AE_1l^2E_2))\\
& -\frac{96}{(1+E_2+E_1+AE_1E_2)^5}((2\,k^3\sqrt{6}E_1+2\,l^3\sqrt{6}E_2+4\,(k-l)^2\sqrt{6}kE_1E_2\\
& +4\,(k-l)^2E_1\sqrt{6}lE_2+A(2\,l^2\sqrt{6}kE_1+2\,k^2\sqrt{6}lE_2)E_1E_2\\
& +2\,A(l^2E_1+k^2E_2)\sqrt{6}kE_1E_2+2\,A(l^2E_1+k^2E_2)E_1\sqrt{6}lE_2)(2\,\sqrt{6}lE_2\\
& +2\,\sqrt{6}kE_1+2\,A\sqrt{6}kE_1E_2+2\,AE_1\sqrt{6}lE_2)^3)\\
& +\frac{72}{(1+E_2+E_1+AE_1E_2)^4}((2\,k^3\sqrt{6}E_1+2\,l^3\sqrt{6}E_2+4\,(k-l)^2\sqrt{6}kE_1E_2
\end{aligned}
$$

$$
\begin{aligned}
&+4\,(k-l)^2E_1\sqrt{6}lE_2+A(2\,l^2\sqrt{6}kE_1+2\,k^2\sqrt{6}lE_2)E_1E_2\\
&+2\,A(l^2E_1+k^2E_2)\sqrt{6}kE_1E_2\\
&+2\,A(l^2E_1+k^2E_2)E_1\sqrt{6}lE_2)(2\,\sqrt{6}lE_2+2\,\sqrt{6}kE_1+2\,A\sqrt{6}kE_1E_2\\
&+2\,AE_1\sqrt{6}lE_2)(24\,l^2E_2+24\,k^2E_1+24\,Ak^2E_1E_2+48\,AkE_1lE_2\\
&+24\,AE_1l^2E_2))-\frac{8}{(1+E_2+E_1+AE_1E_2)^3}((2\,k^3\sqrt{6}E_1+2\,l^3\sqrt{6}E_2\\
&+4\,(k-l)^2\sqrt{6}kE_1E_2+4\,(k-l)^2E_1\sqrt{6}lE_2+A(2\,l^2\sqrt{6}kE_1+2\,k^2\sqrt{6}lE_2)E_1E_2\\
&+2\,A(l^2E_1+k^2E_2)\sqrt{6}kE_1E_2\\
&+2\,A(l^2E_1+k^2E_2)E_1\sqrt{6}lE_2)(48\,l^3\sqrt{6}E_2+48\,k^3\sqrt{6}E_1+48\,Ak^3\sqrt{6}E_1E_2\\
&+144\,Ak^2E_1\sqrt{6}lE_2+144\,AkE_1l^2\sqrt{6}E_2+48\,AE_1l^3\sqrt{6}E_2))\\
&+\frac{120}{(1+E_2+E_1+AE_1E_2)^6}((k^2E_1+l^2E_2+2\,(k-l)^2E_1E_2\\
&+A(l^2E_1+k^2E_2)E_1E_2)(2\,\sqrt{6}lE_2+2\,\sqrt{6}kE_1+2\,A\sqrt{6}kE_1E_2\\
&+2\,AE_1\sqrt{6}lE_2)^4)-\frac{144}{(1+E_2+E_1+AE_1E_2)^5}((k^2E_1+l^2E_2+2\,(k-l)^2E_1E_2\\
&+A(l^2E_1+k^2E_2)E_1E_2)(2\,\sqrt{6}lE_2+2\,\sqrt{6}kE_1+2\,A\sqrt{6}kE_1E_2\\
&+2\,AE_1\sqrt{6}lE_2)^2(24\,l^2E_2+24\,k^2E_1+24\,Ak^2E_1E_2\\
&+48\,AkE_1lE_2+24\,AE_1l^2E_2))+\frac{18}{(1+E_2+E_1+AE_1E_2)^4}((k^2E_1+l^2E_2\\
&+2\,(k-l)^2E_1E_2+A(l^2E_1+k^2E_2)E_1E_2)(24\,l^2E_2+24\,k^2E_1\\
&+24\,Ak^2E_1E_2+48\,AkE_1lE_2+24\,AE_1l^2E_2)^2)\\
&+\frac{24}{(1+E_2+E_1+AE_1E_2)^4}((k^2E_1+l^2E_2+2\,(k-l)^2E_1E_2\\
&+A(l^2E_1+k^2E_2)E_1E_2)(2\,\sqrt{6}lE_2+2\,\sqrt{6}kE_1+2\,A\sqrt{6}kE_1E_2\\
&+2\,AE_1\sqrt{6}lE_2)(48\,l^3\sqrt{6}E_2+48\,k^3\sqrt{6}E_1+48\,Ak^3\sqrt{6}E_1E_2\\
&+144\,Ak^2E_1\sqrt{6}lE_2+144\,AkE_1l^2\sqrt{6}E_2+48\,AE_1l^3\sqrt{6}E_2))\\
&-\frac{2}{(1+E_2+E_1+AE_1E_2)^3}((k^2E_1+l^2E_2+2\,(k-l)^2E_1E_2\\
&+A(l^2E_1+k^2E_2)E_1E_2)(576\,l^4E_2+576\,k^4E_1+576\,Ak^4E_1E_2\\
&+2304\,Ak^3E_1lE_2+3456\,Ak^2E_1l^2E_2+2304\,AkE_1l^3E_2+576\,AE_1l^4E_2)).
\end{aligned}
$$

References

[1] J. Boussinesq, Théorie des ondes et des remous qui se propagent le long d'un canal rectangulaire horizontal, en communiquant au liquide contenu dans ce canal des vitesses sensiblement pareilles de la surface au fond, J. Math. Pures Appl. 17 (1872) 55–108.
[2] D.J. Korteweg, G. de Vries, On the change of form of long waves advancing in a rectangular channel and on a new type of long stationary wave, Philos. Mag. 39 (1895) 422–443.
[3] N.J. Zabusky, M.D. Kruskal, Interaction of solutions in a collisionless plasma and the recurrence of initial states, Phys. Rev. Lett. 15 (1965) 240–243.
[4] R.M. Miura, C.S. Gardner, M.D. Kruskal, Korteweg–de Vries equation and generalizations, II, existence of conservation laws and constants of motion, J. Math. Phys. 9 (1968) 1204–1209.
[5] D.G. Crighton, Applications of KdV, Acta Appl. Math. 39 (1995) 39–67.
[6] G.B. Whitham, Linear and Nonlinear Waves, Wiley, New York, 1974.
[7] A. Ali, H. Kalisch, Energy balance for undular bores, C. R. Mécanique 338 (2010) 67–70.
[8] J.L. Bona, M. Chen, J.-C. Saut, Boussinesq equations and other systems for small-amplitude long waves in nonlinear dispersive media, I: derivation and linear theory, J. Nonlinear Sci. 12 (2002) 283–318.
[9] A. Constantin, The trajectories of particles in Stokes waves, Invent. Math. 166 (2006) 523–535.
[10] A. Constantin, J. Escher, Particle trajectories in solitary water waves, Bull. Amer. Math. Soc. 44 (2007) 423–431.
[11] A. Constantin, M. Ehrnström, G. Villari, Particle trajectories in linear deep-water waves, Nonlinear Anal. Real World Appl. 9 (2008) 1336–1344.
[12] A. Constantin, G. Villari, Particle trajectories in linear water waves, J. Math. Fluid Mech. 10 (2008) 1–18.
[13] M. Ehrnström, G. Villari, Recent progress on particle trajectories in steady water waves, Discrete Contin. Dyn. Syst. Ser. B 12 (2009) 539–559.
[14] H.-K. Chang, Y.-Y. Chen, J.-Ch. Liou, Particle trajectories of nonlinear gravity waves in deep water, Ocean Eng. 36 (2009) 324–329.
[15] R. Grimshaw, The solitary wave in water of variable depth, Part 2, J. Fluid Mech. 46 (1971) 611–622.
[16] J. Fenton, A ninth-order solution for the solitary wave, J. Fluid Mech. 52 (1972) 257–271.
[17] Y.-Y. Chen, H.-C. Hsu, G.-Y. Chen, Lagrangian experiment and solution for irrotational finite-amplitude progressive gravity waves at uniform depth, Fluid Dynam. Res. 42 (2010) 045511. p. 34.

[18] D. Clamond, Steady finite-amplitude waves on a horizontal seabed of arbitrary depth, J. Fluid Mech. 398 (1999) 45–60.
[19] D. Henry, Steady periodic flow induced by the Korteweg–de Vries equation, Wave Motion 46 (2009) 403–411.
[20] A.R. Osborne, A.D. Kirwan, A. Provenzale, L. Bergamasco, The Korteweg–de Vries equation in Lagrangian coordinates, Phys. Fluids 29 (1986) 656–660.
[21] A. Provenzale, A.R. Osborne, G. Boffetta, M. Serio, Particle orbits from the Lagrangian and the Eulerian Korteweg–de Vries equations, Phys. Fluids A2 (1990) 866–869.
[22] A. Constantin, J. Escher, Analyticity of periodic travelling free surface water waves with vorticity, Ann. of Math. 173 (2011) 559–568.
[23] D. Henry, Analyticity of the free surface for periodic travelling capillary-gravity water waves with vorticity, J. Math. Fluid Mech. (2011). http://dx.doi.org/10.1007/s00021-011-0056-z (in print) (online).
[24] D. Henry, Analyticity of the streamlines for periodic travelling free surface capillary-gravity water waves with vorticity, SIAM J. Math. Anal. 42 (2010) 3103–3111.
[25] B.-V. Matioc, Analyticity of the streamlines for periodic traveling water waves with bounded vorticity, Int. Math. Res. Not. 17 (2011) 3858–3871.
[26] M. Bjørkavåg, H. Kalisch, Wave breaking in Boussinesq models for undular bores, Phys. Lett. A 375 (2011) 1570–1578.
[27] W.H. Munk, The solitary wave theory and its application to surf problems, Ann. NY Acad. Sci. 51 (1949) 376–424.
[28] P. Drazin, R.S. Johnson, Solitons: An Introduction, in: Cambridge Texts in Applied Mathematics, Cambridge University Press, Cambridge, 1989.
[29] D.F. Lawden, Elliptic Functions and Applications, Springer, New York, 1989.
[30] R.S. Johnson, A Modern Introduction to the Mathematical Theory of the Water Waves, Cambridge University Press, 1997.